

# An aryl-fused redox-active tetrathiafulvalene with enhanced mixed-valence and radical-cation dimer stabilities

Hendrik V. Schröder,<sup>a</sup> Felix Witte,<sup>a</sup> Marius Gaedke,<sup>a</sup> Sebastian Sobottka,<sup>b</sup> Lisa Suntrup,<sup>b</sup>  
Henrik Hupatz,<sup>a</sup> Arto Valkonen,<sup>c</sup> Beate Paulus,<sup>a</sup> Kari Rissanen,<sup>c</sup> Biprajit Sarkar,<sup>b</sup> and  
Christoph A. Schalley\*<sup>a</sup>

<sup>a</sup> Institut für Chemie und Biochemie, Organische Chemie, Freie Universität Berlin,  
Takustraße 3, 14195 Berlin, Germany.

<sup>b</sup> Institut für Chemie und Biochemie, Anorganische Chemie, Freie Universität Berlin,  
Fabeckstraße 34/36, 14195 Berlin, Germany.

<sup>c</sup> University of Jyväskylä, Department of Chemistry, P.O. Box 35, 40014 Jyväskylä, Finland.

\*Corresponding author e-mail: c.schalley@fu-berlin.de

## Table of contents

1. Experimental details.....	S1
1.1. General methods.....	S1
1.2. Synthesis .....	S1
2. EPR measurements.....	S2
3. UV/Vis-NIR measurements and spectroelectrochemistry.....	S3
4. Electrochemical measurements.....	S7
5. Computational details.....	S8
6. Crystallographic data and electrocrystallisation.....	S9
7. <sup>1</sup> H, <sup>13</sup> C NMR and HR mass spectra.....	S11
8. References.....	S12

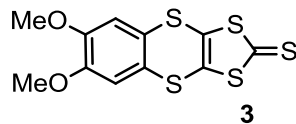
# 1. Experimental details

## 1.1. General Methods

All reagents and solvents were obtained from commercial sources and used without further purification. Dry solvents were purchased from Acros Organics. 6,7-Dimethoxy-1,3-dithiolo[4,5-*b*][1,4]benzodithiin-2-thione (**3**) was synthesised according to a literature procedure.<sup>1</sup> Thin-layer chromatography was performed on silica gel-coated plates with fluorescent indicator F254 (Merck). For column chromatography, silica gel (0.04-0.063 mm, Merck) was used. <sup>1</sup>H and <sup>13</sup>C NMR experiments were performed on a JEOL ECX 400 or a Bruker AVANCE 700 instrument. Solvent residue signals were used as the internal standard. All shifts are reported in ppm and NMR multiplicities are abbreviated as s (singlet), d (doublet), t (triplet), m (multiplet) and br (broad). Coupling constants *J* are reported in Hertz. High-resolution ESI mass spectra were measured on an Agilent 6210 ESI-TOF device (Agilent Technologies). Melting points were determined on a SMP 30 (Stuart) instrument and are uncorrected.

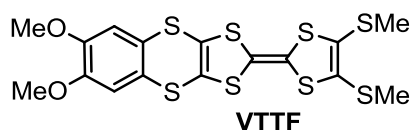
## 1.2. Synthesis

### 6,7-Dimethoxy-1,3-dithiolo[4,5-*b*][1,4]benzodithiin-2-thione (**3**)



Under argon atmosphere, 1,2-diiodo-4,5-dimethoxybenzene (470 mg, 1.20 mmol), bis(tetrabutylammonium) bis(1,3-dithiole-2-thione-4,5-dithiolato)zinc (540 mg, 0.57 mol), Cu<sub>2</sub>O (16 mg, 0.11 mmol), ethyl acetoacetate (30 μL, 0.23 mmol) and *N,N*-dimethylformamide (5.7 mL) were placed into a flame-dried Schlenk tube and the mixture was stirred at 80 °C overnight. Afterwards, the mixture was diluted with CH<sub>2</sub>Cl<sub>2</sub> (50 mL) and washed with water (3x50 mL) and brine (50 mL). The organic phase was dried over MgSO<sub>4</sub> and the residue was purified using column chromatography (SiO<sub>2</sub>, pentane/CH<sub>2</sub>Cl<sub>2</sub> 1:1, *R<sub>f</sub>* ≈ 0.30). The crude product was recrystallised from acetonitrile and CHCl<sub>3</sub> to give thione **3** as yellow crystals (260 mg, 0.78 mmol, 65%). <sup>1</sup>H NMR (400 MHz, CDCl<sub>3</sub>, 298 K): δ = 6.95 (s, 2H, H<sub>Ar</sub>), 3.89 (s, 6H, OMe) ppm. <sup>1</sup>H NMR data are consistent with literature.<sup>1</sup>

## 2-(4,5-Bis(methylthio)-1,3-dithiol-2-ylidene)-6,7-dimethoxybenzo[*b*][1,3]dithiolo[4,5-*e*][1,4]dithiine (VTTF)



6,7-Dimethoxy-1,3-dithiolo[4,5-*b*][1,4]benzodithiin-2-thione (**3**) (777 mg, 2.34 mmol) and 4,5-bis(methylthio)-1,3-dithiol-2-one (491 mg, 2.34 mmol) were dispersed in dry triethylphosphite (40 mL) under argon atmosphere. The mixture was heated to 90 °C overnight. After cooling to room temperature, CH<sub>3</sub>OH (80 mL) was added and the flask was placed in a freezer for 3 days. The precipitate was filtered off and purified by column chromatography (SiO<sub>2</sub>, pentane/CH<sub>2</sub>Cl<sub>2</sub> = 1:1). The product was recrystallised twice, from CH<sub>3</sub>CN and CHCl<sub>3</sub>, to give the desired product as yellow crystals (419 mg, 0.85 mmol, 36%). *R*<sub>f</sub> = 0.25 in pentane/CH<sub>2</sub>Cl<sub>2</sub> = 1:1; m. p. 197 °C; <sup>1</sup>H NMR (700 MHz, CD<sub>2</sub>Cl<sub>2</sub>, 298 K): δ = 6.92 (s, 2H, H<sub>Ar</sub>), 3.82 (s, 6H, OMe), 2.42 (s, 6H, SMe) ppm; <sup>13</sup>C NMR (176 MHz, CD<sub>2</sub>Cl<sub>2</sub>): δ = 150.0, 128.0, 126.5, 124.1, 116.7, 113.4, 112.4, 56.7, 19.6 ppm; ESI-HRMS: *m/z* calcd. for C<sub>16</sub>H<sub>14</sub>O<sub>2</sub>S<sub>8</sub>: 516.8652 [M+Na]<sup>+</sup>, found: 516.8666.

## 2. EPR measurements

CW EPR spectra at X-band frequency (ca. 9.5 GHz) were obtained with a Magnettech MS-5000 benchtop EPR spectrometer equipped with a rectangular TE 102 cavity and TC HO4 temperature controller. The measurements were carried out in synthetic quartz glass tubes. Dry and freshly distilled CH<sub>3</sub>CN was used. Sample preparation and measurements were performed under nitrogen atmosphere. For the preparation of the radical-cation **VTTF**<sup>•+</sup>, 1.0 equiv. of Fe(ClO<sub>4</sub>)<sub>3</sub> was added to a CH<sub>3</sub>CN solution of **VTTF** (0.20 mM). The solution turned immediately dark brown because of the absorption of the radical-cation **VTTF**<sup>•+</sup>. We followed the procedure of EPR radical-cation dimerisation experiments reported elsewhere.<sup>2</sup> Briefly, the EPR signal intensity, measured at different temperatures by integration, was used to calculate the monomer fraction α<sub>M</sub>. The α<sub>M</sub> value decreases with lower temperatures due to the formation of the EPR-silent radical-cation dimer (**VTTF**<sup>•+</sup>)<sub>2</sub>. For the correction of Curie law effects, 2,2,6,6-tetramethylpiperidinyloxy (TEMPO) was used as reference. The experimental α<sub>M</sub> values were fitted with Origin Pro 8 (OriginLab) according to equation 1:

$$\alpha_M = -1 + \frac{\sqrt{1 + 8e^{\left(\frac{-H+T \cdot S}{RT}\right)} [\text{VTTF}^{\bullet+}]}}{4e^{\left(\frac{-H+T \cdot S}{RT}\right)} [\text{VTTF}^{\bullet+}]} \quad \text{eq. (1)}$$

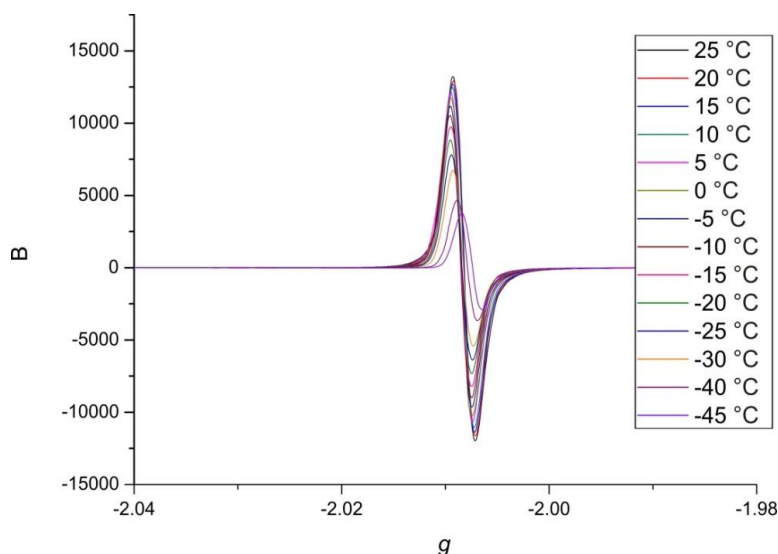


**Fig. S1** EPR signal of **VTTF<sup>•+</sup>** (0.20 mM, CH<sub>3</sub>CN) at different temperatures. No precipitation was observed irrespective of the temperature.

### 3. UV/Vis-NIR measurements and spectroelectrochemistry

UV/Vis spectra of **VTTF** were recorded on a Cary 50 Bio photospectrometer (Varian) equipped with a xenon lamp. UV/Vis-NIR measurements were performed on an Avantes spectrometer with an AvaLight-DH-S-Bal light source, an AvaSpec-ULS2048 UV/Vis detector, and an AvaSpec-NIR256-TEC NIR detector. CH<sub>3</sub>CN and CH<sub>2</sub>Cl<sub>2</sub> with HPLC grade and Suprasil glass cuvettes with a path-length of 1, 0.5 or 0.1 cm were used. Spectroelectrochemical measurements were carried out in an optically transparent thin-layer electrochemical (OTTLE) cell (CaF<sub>2</sub> windows) with a platinum-mesh working electrode, a platinum-mesh counter electrode, and a silver-foil pseudoreference electrode. Voltammetric cycles between 0 and 1 V (vs silver pseudoreference) were performed.

Due to the low solubility of neutral **VTTF** in CH<sub>3</sub>CN, a photometric titration to investigate the mixed-valence dimer was done in CH<sub>2</sub>Cl<sub>2</sub>. Addition of neutral **VTTF** to previously generated **VTTF<sup>•+</sup>** leads to an emergent weak band (> 1300 nm) with no clear maximum as shown in Fig. S4. The rather unstructured and weak NIR band may at first sight come as a surprise. However, this characteristic band was also observed in spectroelectrochemistry measurements and in a CH<sub>2</sub>Cl<sub>2</sub>/CH<sub>3</sub>CN mixture (1:1) as shown in Fig. S5. Furthermore, mixed-valence complexes of tetrathiafulvalene which exhibit very similar charge resonance bands were previously reported.<sup>3-5</sup> The binding constant of the

mixed-valence complex  $(\mathbf{VTTF}_2)^{\bullet+}$   $K_{MV}$  in  $\text{CH}_2\text{Cl}_2$  was obtained by non-linear curve fitting of a 1:1 binding model as described earlier<sup>6</sup> with the program Origin Pro (OriginLab) according to equation 2 taking the dilution of  $[\mathbf{VTTF}^{\bullet+}]_0$  into account. The binding constant  $K_{MV}$  was averaged from the fit of four different wavelengths (1600, 1800, 2000, and 2200 nm).

$$\Delta A_{obs} = \epsilon \frac{1}{2} \left( [\mathbf{VTTF}]_0 + [\mathbf{VTTF}^{\bullet+}]_0 + \frac{1}{K_{MV}} - \sqrt{\left([\mathbf{VTTF}]_0 + [\mathbf{VTTF}^{\bullet+}]_0 + \frac{1}{K_{MV}}\right)^2 + 4[\mathbf{VTTF}]_0[\mathbf{VTTF}^{\bullet+}]_0} \right) \quad \text{eq. (2)}$$

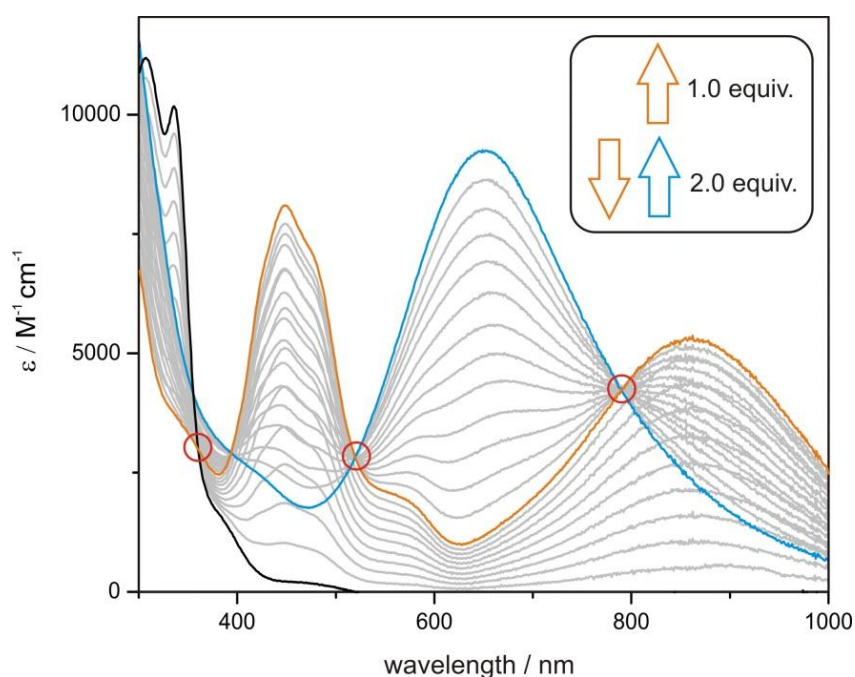


**Fig. S2** Photometric UV/Vis titration of **VTTF** ( $5 \cdot 10^{-5}$  M,  $\text{CH}_3\text{CN}$ , 298 K) with one-electron oxidant  $\text{Fe}(\text{ClO}_4)_3$ . The black curve corresponds to neutral **VTTF** (0.0 equiv. oxidant), the orange curve to its radical-cation **VTTF**<sup>•+</sup> (1.0 equiv. oxidant) and the blue curve to the fully oxidised dication **VTTF**<sup>2+</sup> (2.0 equiv. oxidant). The clear-cut isosbestic points (red circles) confirm a clean transition between all three oxidation states.

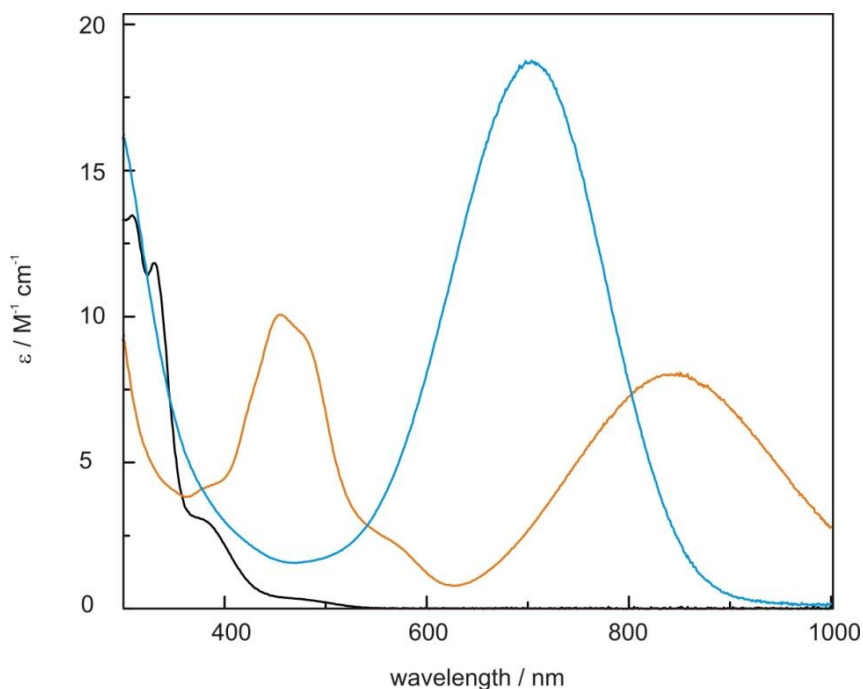


**Fig. S3** UV/Vis spectra ( $5 \cdot 10^{-5}$  M,  $\text{CH}_3\text{CN}$ , 298 K) of **TMT-TTF** in oxidation state 0 (black), +1 (orange), and +2 (blue). The oxidised species were generated by addition of  $\text{Fe}(\text{ClO}_4)_3$ .

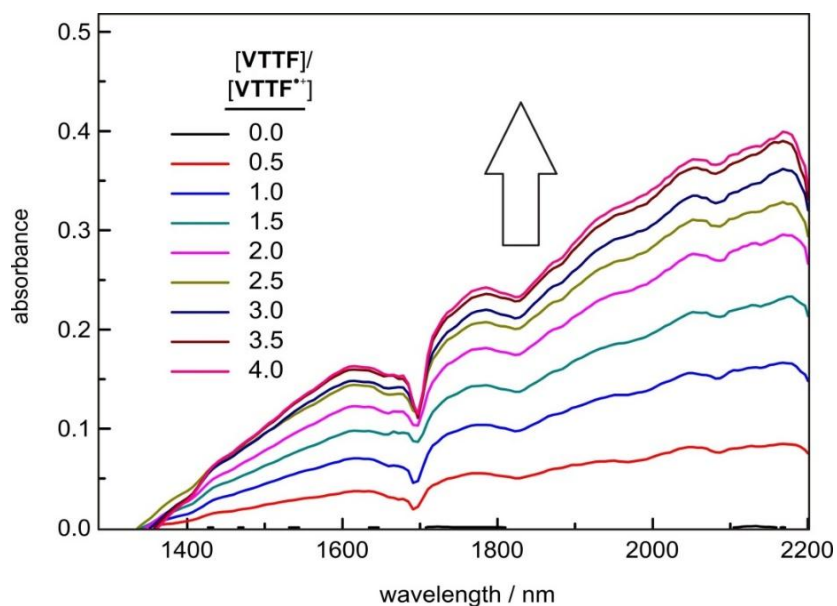


**Fig. S4** Photometric NIR titration of  $\text{VTTF}^{*\cdot+}$  (5.0 mM,  $\text{CH}_2\text{Cl}_2$ , 298 K) with a concentrated  $\text{CH}_2\text{Cl}_2$  solution (50 mM) of neutral  $\text{VTTF}$ . The emerging broad band  $> 1300$  nm is caused by the formation of the mixed-valence  $(\text{VTTF}_2)^{*\cdot+}$  dimer.

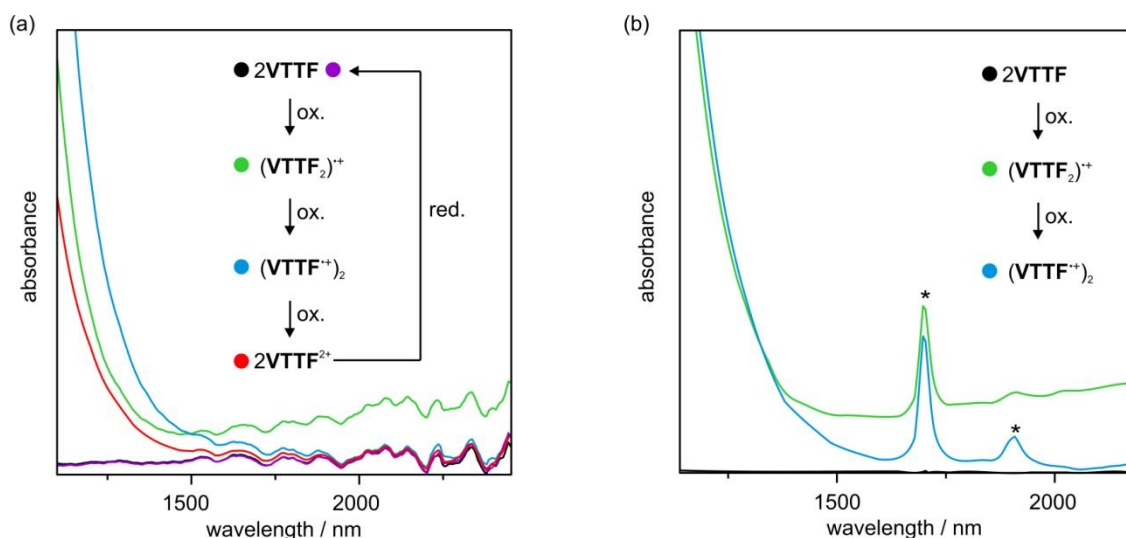


**Fig. S5** (a) Changes of the NIR spectra of **VTTF** (30 mM, CH<sub>2</sub>Cl<sub>2</sub>, 298 K, 0.1 M *n*-Bu<sub>4</sub>NPF<sub>6</sub>) in the course of stepwise oxidation and reduction during spectroelectrochemistry. The results shows that only the mixed-valence state displays the broad NIR band > 1300 nm and that the oxidation/reduction process is fully reversible. (b) Changes of the NIR spectra during stepwise chemical oxidation of **VTTF** (30 mM, CH<sub>2</sub>Cl<sub>2</sub>/CH<sub>3</sub>CN (1:1), 298 K) by addition of chemical oxidant Fe(ClO<sub>4</sub>)<sub>3</sub>. Artefacts are marked with an asterisk.

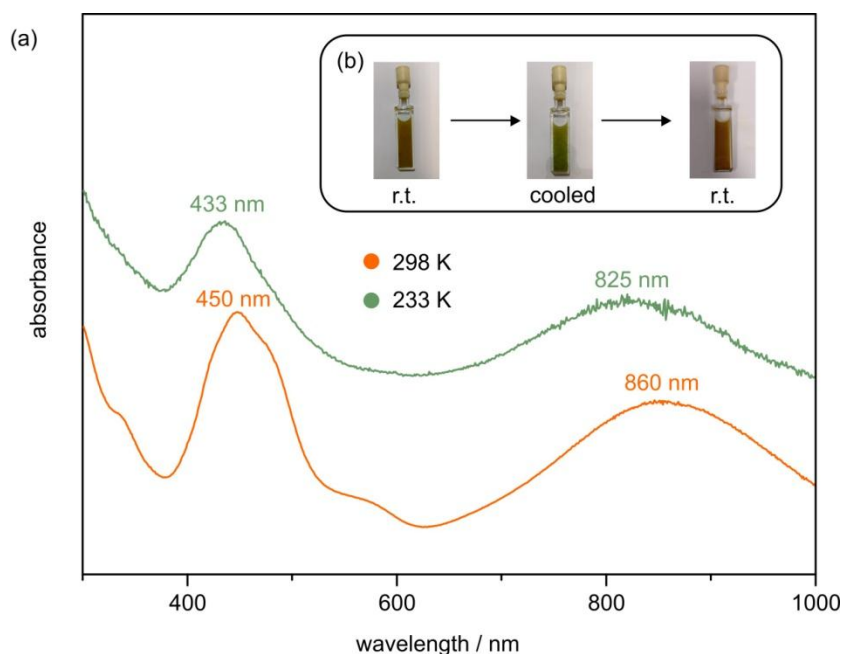


**Fig. S6** (a) UV/Vis spectra (25 mM, CH<sub>3</sub>CN,) of **VTTF**<sup>•+</sup> at room temperature and 233 K. The oxidised monomeric **VTTF**<sup>•+</sup> was chemically generated by addition of 1 equiv. Fe(ClO<sub>4</sub>)<sub>3</sub>. The broadening of bands for the 233 K measurement is due to slight precipitation in the cuvette. (b) Photographs of the cuvette before cooling, directly after cooling, and after warming up again to room temperature.

## 4. Electrochemical measurements

Cyclic Voltammetry (CV) and differential pulse Voltammetry (DPV) were performed on a PGSTAT302N potentiostat (Autolab) using a three-electrode configuration: a freshly polished glassy carbon working electrode, a platinum wire counter electrode and a silver wire pseudoreference electrode. All measurements were conducted twice, CV measurements in addition with a broad range of different scan rates ( $25 \rightarrow 1000 \text{ mV s}^{-1}$ ) to ensure reversibility of the processes. The decamethylferrocene/decamethylferrocenium couple was used as the internal reference. Potentials were referenced against the ferrocene/ferrocenium ( $\text{FcH}/\text{FcH}^+$ ) couple.<sup>7</sup> Dry and argon-purged solvents were used.

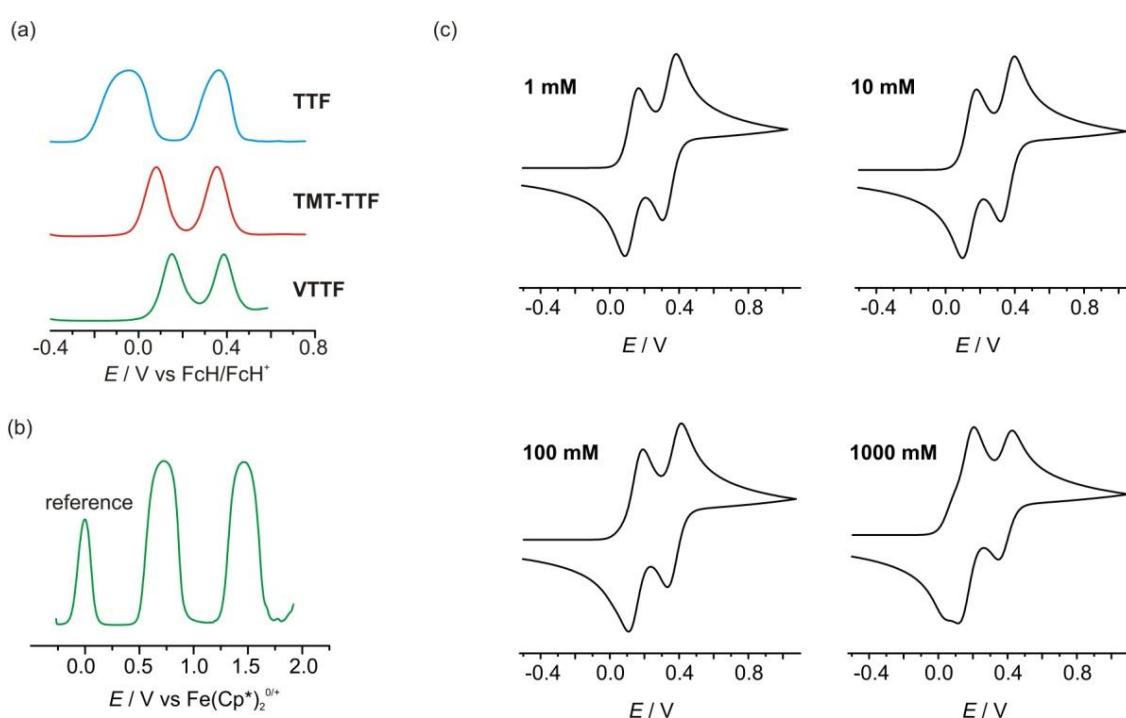


**Fig. S7** (a) DPV measurements ( $10 \text{ mV s}^{-1}$  scan rate,  $25 \text{ mV}$  modulation amplitude,  $50 \text{ ms}$  modulation time,  $5 \text{ mV}$  step potential,  $0.5 \text{ s}$  interval time) of **TTF**, **TMT-TTF** and **VTTF** ( $0.1 \text{ mM}$ ) in  $\text{CH}_3\text{CN}$  ( $0.1 \text{ M } n\text{-Bu}_4\text{NPF}_6$ ). (b) DPV measurements ( $10 \text{ mV s}^{-1}$  scan rate,  $25 \text{ mV}$  modulation amplitude,  $50 \text{ ms}$  modulation time,  $5 \text{ mV}$  step potential,  $0.5 \text{ s}$  interval time) of **VTTF** ( $22 \text{ mM}$ ) in  $\text{CH}_2\text{Cl}_2$  ( $0.1 \text{ M}$  tetrabutylammonium tetrakis[3,5-bis(trifluoromethyl)phenyl]borate). (c) Simulated voltammograms ( $100 \text{ mV s}^{-1}$ ) for different initial concentrations of monomer **VTTF**. Note that a broadening/splitting of the first redox wave emerges in the molar concentration range.

Regarding the voltammetric behavior of **VTTF**, mixed-valence complexes, for example covalently<sup>8</sup> or strongly non-covalently bound (e.g.  $K_{MV} = 10^4 \text{ M}^{-1}$ )<sup>9</sup> organic redox-active molecules, usually show a splitting or at least a broadening of the first redox-wave. However, even in more concentrated  $\text{CH}_2\text{Cl}_2$  solution (Fig. S7b) using tetrabutylammonium



tetrakis[3,5-bis(trifluoromethyl)phenyl]borate as weakly-coordinating<sup>10</sup> electrolyte, we could not observe a distinct splitting of the first transition. To unravel, why this is not observed for **VTTF** and its corresponding mixed-valence complex (**VTTF<sub>2</sub>**)<sup>•+</sup>, we conducted digital simulations (DigiElch Professional software package)<sup>11</sup> based on the determined redox-potentials and equilibrium constants which are depicted in Figure S7c. We estimate that a broadening effect of the first wave could emerge in the molar range. Common measuring concentrations and a window for reliable data for our CV and DPV set up is approximately 0.1-20 mM analyte concentration. The absence of visible features in the voltammograms does not exclude partial presence of the mixed-valence dimer in solution.

## 5. Computational details

Structure optimisations of **VTTF** and its dimers in their 0, 1+, and 2+ charge state at the TPSS-D3(BJ)/def2-TZVP<sup>12-15</sup> level of DFT employing the RI-J approximation<sup>16</sup> for the Coulomb term and COSMO<sup>17</sup> ( $\epsilon = 36.6$ ) for simulating implicit solvent effects were performed using the Turbomole 7.0.1<sup>18</sup> programme package. Minima were ascertained by frequency analyses showing no imaginary frequencies. Most of the subsequent single point calculations were done at the PBE0-D3(BJ)/def2-TZVP<sup>19</sup> level employing the RIJCOSX<sup>20</sup> approximation and incorporating implicit solvent effects with CPCM ( $\epsilon = 36.6$ )<sup>21</sup> using ORCA 4.0.0.<sup>22</sup> These included the computation of the spin densities of (**VTTF<sub>2</sub>**)<sup>•+</sup> and **VTTF**<sup>•+</sup> (Fig. S7) and the prediction of UV/Vis absorption spectra in the framework of linear-response time-dependent DFT (Fig. 4). Furthermore, free enthalpies of association  $\Delta G_a$  were calculated according to

$$\Delta G_a = \Delta E + \Delta G_{RRHO} + \Delta G_{solv}$$

where  $\Delta E$  is the electronic binding energy of the dimer calculated *in vacuo* at the PBE0-D3(BJ)/def2-QZVP<sup>23</sup> level. Note that the BSSE is not accounted for, since the quadruple-zeta basis set is assumed to be near the basis set limit for these kinds of DFT calculations.<sup>24</sup>  $\Delta G_{RRHO}$  was obtained from calculated frequencies using standard statistical thermodynamic approaches, whereas low-lying vibrational modes were corrected via the so-called *rigid-rotor harmonic-oscillator ansatz* proposed by Grimme.<sup>25</sup> The last term,  $\Delta G_{solv}$ , represents the contribution from the dissolution of the dimer in comparison to two dissolved monomers.  $\Delta G_{solv}$  was computed with the COSMOTermX programme suite<sup>26,27</sup> applying the COSMO-RS scheme<sup>28,29</sup> with BP86/def-TZVP<sup>30-32</sup> parametrisation. Table S1 summarises the various contributions to  $\Delta G_a$  for both (**VTTF<sub>2</sub>**)<sup>•+</sup> and (**VTTF**<sup>•+</sup>)<sub>2</sub>. Discrepancies between the two dimers are explained by electrostatic repulsions in the gas-phase present in (**VTTF**<sup>•+</sup>)<sub>2</sub> and a significant charge stabilisation in solution.

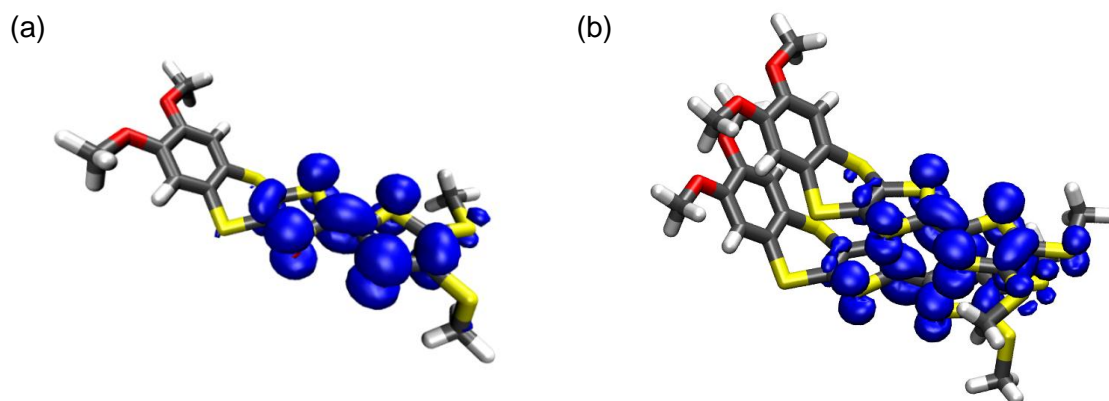


**Fig. S8** Spin density of (a)  $\text{VTTF}^{\bullet+}$  and (b)  $(\text{VTTF}_2)^{\bullet+}$  dimer obtained at the PBE0-D3(BJ)/def2-TZVP level of DFT.

**Table S1** Contributions to the free enthalpies of association,  $\Delta G_a$ , data given in  $\text{kJ mol}^{-1}$ .

	$\Delta E$	$\Delta G_{\text{RRHO}}$	$\Delta G_{\text{solv}}$	$\Delta G_a$
$(\text{VTTF}_2)^{\bullet+}$	-144.7	86.3	54.2	- 4.3
$(\text{VTTF}^{\bullet+})_2$	62.4	88.1	-136.8	13.6

## 6. Crystallographic data and electrocrystallisation

The electrocrystallisation of  $[\text{VTTF}](\text{BF}_4)_2$  was conducted using a custom made H-cell which consists of two glass compartments separated by a glass frit. A solution of 12 mg (24  $\mu\text{mol}$ , 12  $\mu\text{mol}$  per compartment) **VTTF** and 100 mg (0.3 mmol)  $n\text{-Bu}_4\text{NBF}_4$  in  $\text{CH}_2\text{Cl}_2$  (20 mL) was distributed equally to both compartments. After closing the apparatus with two septa, a platinum wire was submerged into the solution in each compartment. The wires then acted as the electrodes for a self-made constant current source. A current of 1  $\mu\text{A}$  was applied over 10 days, until a black solid appeared on the anode, from which a dark green crystal of a  $[\text{VTTF}](\text{BF}_4)_2$  salt suitable for X-ray diffraction could be harvested. The applied current and the duration of electrolyses (0.86 C = 8.96  $\mu\text{mol}$ ) are not sufficient to quantitatively oxidise **VTTF** in solution to the corresponding dication  $\text{VTTF}^{2+}$ . However by turning brown, the solution indicated the formation of a partly soluble radical-cationic species. Due to the non-polar nature of  $\text{CH}_2\text{Cl}_2$  and most certainly a lower solubility of the fully oxidised  $\text{VTTF}^{2+}$ , we assume that the dication precipitates at the anode and, thus, is removed from the electrochemical disproportionation equilibrium according to an  $EEC_1$  mechanism.

The data for  $[\text{VTTF}](\text{BF}_4)_2$  were collected on an Agilent SuperNova single-source diffractometer equipped with an Eos CCD detector at 120(2) K using mirror-monochromated Mo- $K\alpha$  ( $\lambda = 0.71073 \text{ \AA}$ ) radiation. Data collection and reduction was performed using the program *CrysAlisPro*.<sup>33</sup> The analytical face-indexing-based absorption correction method was

applied. The structure was solved by intrinsic phasing methods (*SHELXT*<sup>34</sup>) and refined by full-matrix least squares on  $F^2$  using *WinGX*<sup>35</sup> which utilises the *SHELXL-2017/1*<sup>36</sup> module. All hydrogen atoms were constrained to their idealised positions and refined using riding models with  $U_{eq}(H)$  of  $1.5U_{eq}(C)$  for terminal methyl groups, and of 1.2 of  $U_{eq}(C)$  for other groups.

Crystal data of **[VTTF](BF<sub>4</sub>)<sub>2</sub>**: C<sub>16</sub>H<sub>14</sub>B<sub>2</sub>F<sub>8</sub>O<sub>2</sub>S<sub>8</sub>,  $M = 668.37$ , monoclinic, space group  $P2_1/n$  (no.14),  $a = 10.7366(4)$ ,  $b = 11.0614(5)$ ,  $c = 21.0424(11)$  Å,  $\beta = 101.460(4)^\circ$ ,  $V = 2449.2(2)$  Å<sup>3</sup>,  $Z = 4$ ,  $\rho_{calc} = 1.813$  Mgm<sup>-3</sup>,  $\mu = 0.807$  mm<sup>-1</sup>,  $F(000) = 1344$ ,  $\theta$  range = 2.98-29.81°, 10396 reflections collected, 6081 unique ( $R_{int} = 0.0275$ ,  $I > 2\sigma(I) = 4696$ ), which were used in all calculations (329 parameters), Goodness-of-fit ( $F^2$ ) = 1.025. The final  $R$  indices [ $I > 2\sigma(I)$ ]:  $R1 = 0.0386$  and  $wR2 = 0.0800$ .  $R$  indices (all data):  $R1 = 0.0578$  and  $wR2 = 0.0892$ . Largest residual electron densities: 0.435 and -0.359 e.Å<sup>-3</sup>.

X-ray data of neutral **VTTF** were collected on a Bruker D8 Venture system at 100(2) K using graphite-monochromated Cu<sub>K $\alpha$</sub>  radiation ( $\lambda_\alpha = 1.54178$  Å). The strategy for the data collection was evaluated by using the *APEX2* software.<sup>37</sup> The data were collected by the standard omega + phi scan techniques, and were scaled and reduced using *Saint+* and *SADABS* software.<sup>38,39</sup> The structures were solved by intrinsic phasing methods using *SHELXT-2014/7*.<sup>34</sup> Structures were refined by full matrix least-squares using *SHELXL-2014/7*, refining on  $F^2$ .<sup>36,40</sup> Non-hydrogen atoms were refined anisotropically.

Crystal data of **VTTF**: C<sub>16</sub>H<sub>14</sub>O<sub>2</sub>S<sub>8</sub> ( $M = 494.75$  g/mol): monoclinic, space group  $P2_1/c$  (no. 14),  $a = 31.7792(12)$  Å,  $b = 4.5304(2)$  Å,  $c = 14.5020(6)$  Å,  $\beta = 101.1090(10)^\circ$ ,  $V = 2048.77(15)$  Å<sup>3</sup>,  $Z = 4$ ,  $T = 100(2)$  K,  $\mu(CuK\alpha) = 8.164$  mm<sup>-1</sup>,  $\rho_{calc} = 1.604$  g/cm<sup>3</sup>, 17424 reflections measured ( $8.506^\circ \leq 2\theta \leq 144.864^\circ$ ), 4028 unique ( $R_{int} = 0.0368$ ,  $R_{sigma} = 0.0319$ ) which were used in all calculations. The final  $R1$  was 0.0302 ( $I > 2\sigma(I)$ ) and  $wR2$  was 0.0836 (all data). Largest residual electron densities: 0.49 and -0.33 e.Å<sup>-3</sup>.

## 7. $^1\text{H}$ , $^{13}\text{C}$ NMR and HR mass spectra

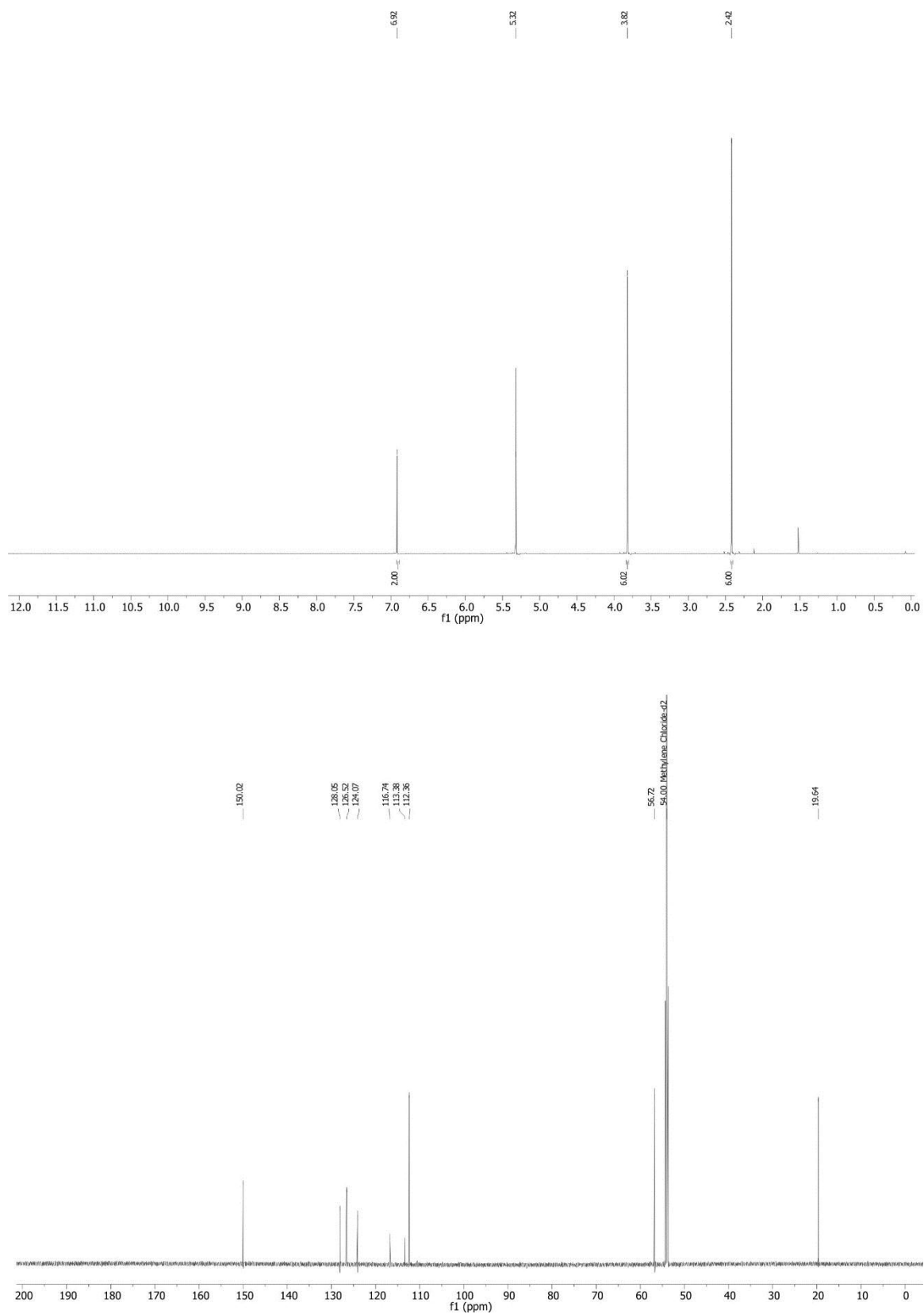


**Fig. S9**  $^1\text{H}$  (top) and  $^{13}\text{C}$  (bottom) NMR spectrum (700/176 MHz,  $\text{CD}_2\text{Cl}_2$ , 298 K) of VTTF.

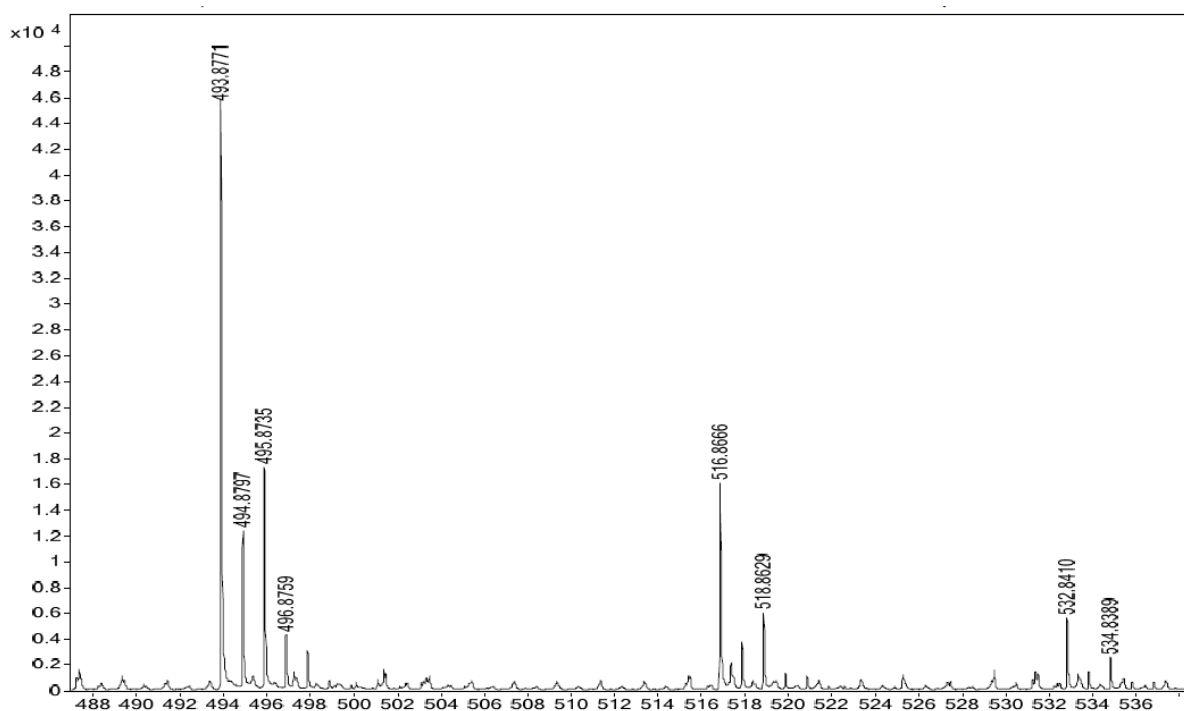


**Fig. S10** ESI high-resolution mass spectrum of **VTTF** (positive mode, MeOH).

## 8. References

- 1 J. Sun, X. Lu, J. Shao, Z. Cui, Y. Shao, G. Jiang, W. Yu and X. Shao, *RSC Adv.*, 2013, **3**, 10193.
- 2 J. M. Lu, S. V. Rosokha and J. K. Kochi, *J. Am. Chem. Soc.*, 2003, **125**, 12161.
- 3 G. Barin, A. Coskun, D. C. Friedman, M. a Olson, M. T. Colvin, R. Carmielli, S. K. Dey, O. A. Bozdemir, M. R. Wasielewski and J. F. Stoddart, *Chem. Eur. J.*, 2011, **17**, 213.
- 4 A. Coskun, J. M. Spruell, G. Barin, A. C. Fahrenbach, R. S. Forgan, M. T. Colvin, R. Carmielli, D. Benitez, E. Tkatchouk, D. C. Friedman, A. A. Sarjeant, M. R. Wasielewski, W. A. Goddard III and J. F. Stoddart, *J. Am. Chem. Soc.*, 2011, **133**, 4538-4547.
- 5 M. Hasegawa, J.-I. Takano, H. Enozawa, Y. Kuwatani and M. Iyoda, *Tetrahedron Lett.*, 2004, **45**, 4109.
- 6 P. Thordarson, *Chem. Soc. Rev.*, 2011, **40**, 1305.
- 7 J. R. Aranzaes, M.-C. Daniel and D. Astruc, *Can. J. Chem.*, 2006, **84**, 288.
- 8 M. Hasegawa, K.-I. Nakamura, S. Tokunaga, Y. Baba, R. Shiba, T. Shirahata, Y. Mazaki and Y. Misaki, *Chem. Eur. J.*, 2016, **22**, 10090.
- 9 M. A. Christensen, C. R. Parker, T. J. Sørensen, S. de Graaf, T. J. Morsing, T. Brock-Nannestad, J. Bendix, M. M. Haley, P. Rapta, A. Danilov, S. Kubatkin, O. Hammerich and M. B. Nielsen, *J. Mater. Chem. C*, 2014, **2**, 10428.
- 10 W. E. Geiger and F. Barrière, *Acc. Chem. Res.*, 2010, **43**, 1030.

- 11 DigiElch Professional Version 7.FD 2006, ElchSoft GbR, Kleinromstedt, Germany.
- 12 J. Tao, J. P. Perdew, V. N. Staroverov and G. E. Scuseria, *Phys. Rev. Lett.*, 2003, **91**, 146401.
- 13 S. Grimme, J. Antony, S. Ehrlich and H. Krieg, *J. Chem. Phys.*, 2010, **132**, 154104.
- 14 S. Grimme, S. Ehrlich and L. Goerigk, *J. Comput. Chem.*, 2011, **32**, 1456.
- 15 K. Eichkorn, F. Weigend, O. Treutler and R. Ahlrichs, *Theor. Chem. Acc.*, 1997, **97**, 119.
- 16 K. Eichkorn, O. Treutler, H. Öhm, M. Häser and R. Ahlrichs, *Chem. Phys. Lett.*, 1995, **240**, 283.
- 17 A. Klamt and G. Schüürmann, *J. Chem. Soc., Perkin Trans. 2*, 1993, 799.
- 18 R. Ahlrichs, M. Bär, M. Häser, H. Horn and C. Kölmel, *Chem. Phys. Lett.*, 1989, **162**, 165.
- 19 J. P. Perdew, M. Ernzerhof and K. Burke, *J. Chem. Phys.*, 1996, **105**, 9982.
- 20 F. Neese, F. Wennmohs, A. Hansen and U. Becker, *Chem. Phys.*, 2009, **356**, 98.
- 21 V. Barone and M. Cossi, *J. Phys. Chem. A* 1998, **102**, 1995.
- 22 F. Neese, *Wiley Interdiscip. Rev. Comp. Mol. Sci.*, 2012, **2**, 73.
- 23 F. Weigand and R. Ahlrichs, *Phys. Chem. Chem. Phys.* 2005, **7**, 3297.
- 24 C. J. Cramer, *Essentials of computational chemistry: theories and models*, Wiley, Chichester, West Sussex, England; Hoboken, NJ, 2<sup>nd</sup> edition, **2004**.
- 25 S. Grimme, *Chem. Eur. J.*, 2012, **18**, 9955.
- 26 COSMOtherm, C3.0, release 1602, COSMOlogic GmbH & Co KG, <http://www.cosmologic.de>
- 27 F. Eckert and A. Klamt, *AIChE J*, 2002, **48**, 369.
- 28 A. Klamt, *J. Phys. Chem.*, 1995, **99**, 2224.
- 29 A. Klamt, V. Jonas, T. Bürger and J. C. Lohrenz, *J. Phys. Chem. A*, 1998, **102**, 5074.
- 30 A. D. Becke, *Phys. Rev. A*, 1988, **38**, 3098.
- 31 J. P. Perdew, *Phys. Rev. B*, 1986, **33**, 8822.
- 32 A. Schäfer, C. Huber and R. Ahlrichs, *J. Chem. Phys.*, 1994, **100**, 5829.
- 33 *CrysAlisPro* (Version 1.171.38.41.), Rigaku Oxford Diffraction, 2015.
- 34 G. M. Sheldrick, *Acta Crystallogr., Sect. A: Found. Adv.*, 2015, **71**, 3.
- 35 L. J. Farrugia, *J. Appl. Crystallogr.*, 2012, **45**, 849.
- 36 G. M. Sheldrick, *Acta Crystallogr., Sect. C: Struct. Chem.*, 2015, **71**, 3.
- 37 Bruker, APEX2, Bruker AXS Inc., Madison, WI, 2012.
- 38 SAINT+ (Data Integration Engine, Version 8.27b), Bruker AXS Inc., Madison, WI, 1997-2012.
- 39 G. M. Sheldrick, SADABS (Ver. 2008/1), Bruker AXS Inc., Göttingen, Germany, 2008.

40 (a) G. M. Sheldrick, *Acta Cryst. Sect A.*, 2008, **64**, 112; (b) C. B. Hübschle, G. M. Sheldrick and B. Dittrich, *J. Appl. Cryst.* 2011, **44**, 1281; (c) G. M. Sheldrick, SHELXL (Version 2014/7), Bruker AXS Inc., Göttingen, Germany, 2014.